TU Delft

Delft University of Technology

Template-free preparation of porous Co microfibers from spent lithium-ion batteries as a promising microwave absorber

Wu, Xiao Min; Xie, Fei; Yao, Yong Lin; Sun, Yue; Hua, Zhong Sheng; Zhao, Zhuo; Yang, Y.

DOI
10.1007/s12598-022-02034-w

Publication date
2022

Document Version
Final published version

Published in
Rare Metals

Citation (APA)
Wu, X. M., Xie, F., Yao, Y. L., Sun, Y., Hua, Z. S., Zhao, Z., & Yang, Y. (2022). Template-free preparation of porous Co microfibers from spent lithium-ion batteries as a promising microwave absorber. *Rare Metals*, *41*(10), 3475-3485. https://doi.org/10.1007/s12598-022-02034-w

Important note
To cite this publication, please use the final published version (if applicable).
Please check the document version above.

Copyright
Other than for strictly personal use, it is not permitted to download, forward or distribute the text or part of it, without the consent of the author(s) and/or copyright holder(s), unless the work is under an open content license such as Creative Commons.

Takedown policy
Please contact us and provide details if you believe this document breaches copyrights.
We will remove access to the work immediately and investigate your claim.

This work is downloaded from Delft University of Technology.
For technical reasons the number of authors shown on this cover page is limited to a maximum of 10.

Green Open Access added to TU Delft Institutional Repository

'You share, we take care!' - Taverne project

https://www.openaccess.nl/en/you-share-we-take-care

Otherwise as indicated in the copyright section: the publisher is the copyright holder of this work and the author uses the Dutch legislation to make this work public.

Rare Met. (2022) 41(10):3475–3485
https://doi.org/10.1007/s12598-022-02034-w

RARE METALS

ORIGINAL ARTICLE

Template-free preparation of porous Co microfibers from spent lithium-ion batteries as a promising microwave absorber

Xiao-Min Wu, Fei Xie, Yong-Lin Yao*, Yue Sun, Zhong-Sheng Hua, Zhuo Zhao*, Yong-Xiang Yang

Received: 23 October 2021 / Revised: 22 December 2021 / Accepted: 17 January 2022 / Published online: 17 July 2022
© Youke Publishing Co., Ltd. 2022

Abstract In order to take full advantage of the secondary resources, in this paper, we reported a template-free process to prepare porous Co microfibers from spent lithium-ion batteries (LIBs). First, the waste $LiCoO_2$ powders were leached by oxalic acid at a suitable temperature, and rod-like cobalt oxalate powders were obtained. Second, the porous Co microfibers were prepared by using the cobalt oxalate as precursors through a thermal decomposition at 420 °C under nitrogen atmosphere. The prepared Co microfibers possess diameters of 1–2 μm, and each microfiber consists of small particles with size of 100–200 nm. The Co microfibers (25 wt%)/paraffin composite exhibited excellent microwave absorption performance. When the sample thickness is 4.5 mm, the reflection losses reach − 36.14 and − 38.20 dB at 4.16 and 17.60 GHz, respectively, and the effective bandwidth reaches up to 5.52 GHz. This indicates that the Co microfibers can be used as a promising microwave absorber. Therefore, this paper demonstrates a novel process to make a high value-added product through recycling from the spent lithium-ion batteries. In addition, it is advantageous to eliminate the hazard of spent lithium-ion batteries and electromagnetic radiation to environment and human health.

Keywords Spent lithium-ion batteries (LIBs); Co microfibers; Recycling; Oxalic acid leaching; Microwave absorption

1 Introduction

In the last few decades, lithium-ion batteries (LIBs) have become the most widely used secondary batteries in many portable electronic devices due to their outstanding properties including high energy density, no memory effect, low self-discharge rate and long cycle life [1–3]. In addition to the traditional field of consumer electronics, there are also large LIBs demands for some new areas, such as new energy vehicles and energy storage [4, 5]. In recent years, the production quantity of LIBs has kept increasing at a high speed due to the huge market demands. For example, the LIBs output of China reached 18 billion units in 2018, which is more than three times the output in 2015. In response to the large usage of LIBs, it is inevitably that a huge quantity of spent LIBs will be produced when the LIBs lose efficacy [6, 7]. Mass of valuable elements exist in the spent LIBs, which are important secondary sources. Meanwhile, some toxic materials like heavy metals, organic electrolytes and binders are serious threats to the ecological environment and people's health [8]. Therefore, it has become an urgent problem to realize the harmlessness and resources circulation of the spent LIBs.

Up to now, various kinds of LIBs have been developed based on different cathode active materials, e.g., $LiCoO_2$

Supplementary Information The online version contains supplementary material available at https://doi.org/10.1007/s12598-022-02034-w.

X.-M. Wu, F. Xie, Y.-L. Yao*, Y. Sun, Z.-S. Hua, Z. Zhao*
Anhui Province Key Laboratory of Metallurgical Engineering & Resources Recycling, School of Metallurgical Engineering, Anhui University of Technology, Maanshan 243002, China
e-mail: yaoyonglin@ahut.edu.cn

Z. Zhao
e-mail: zhaozhuo1018@163.com

Y.-X. Yang
Department of Materials Science and Engineering, Delft University of Technology, Delft 2628CD, Netherlands

[9–11], $LiNi_xCo_yMn_zO_2$ (LNCM) [12, 13] and $LiFePO_4$ [14–16]. For the recovery of the valuable metals from these cathode materials, two strategies were usually employed. In the first way, the valuable metals were recovered one by one through pyrometallurgy or hydrometallurgy processes [4, 17–19]. The pyrometallurgy processes usually suffer from high energy consumption, severe secondary contamination and significant loss of lithium [20]. At present, the hydrometallurgy process is regarded as a preferable approach for the recycling of spent LIBs, and some new selective leaching methods were proposed, such as the selective extraction of lithium by oxalic acid or tartaric acid leaching [21, 22].

In the second way, the transition metals in the spent LIBs were recycled together to prepare oxides, and then the oxides can be used to produce high value-added products such as new cathode materials [23–26]. It is interesting to find that the transition metals Co, Ni, Fe and Mn in the cathode materials are also the main components of microwave absorbing materials. Over the years, in order to eliminate the harm of electromagnetic (EM) radiation to environment and human health, various microwave absorbing materials including Fe [27], Ni [28, 29], Co [30, 31], Co_3O_4 [32], FeNi [33, 34], FeCo [35, 36], MnO_2 [37] and $NiCo_2O_4$ [38] have been extensively studied, and they exhibited excellent microwave absorbing properties. Therefore, it is feasible and meaningful to prepare high value-added microwave absorbing materials from the spent LIBs.

Oxalic acid was often used as leaching agent as well as precipitant to leach the cathode materials, due to that $Li_2C_2O_4$ is soluble, while the leached transition metal ions (Co^{2+}, Ni^{2+}, Mn^{2+}) will combine $C_2O_4^{2-}$ subsequently to form insoluble oxalate precipitates. Sun et al. [21] and Zeng et al. [39] recovered $CoC_2O_4{\cdot}2H_2O$ by using oxalic acid to treat $LiCoO_2$ cathode materials. When the $CoC_2O_4{\cdot}2H_2O$ powders were decomposed by thermal treatment in N_2 atmosphere, Co powders can be obtained [21]. Zhang et al. [40] used oxalic acid to treat $Li(Ni_{1/3}Co_{1/3}Mn_{1/3})O_2$ cathode materials and a complex oxalate $(Ni_{1/3}Co_{1/3}Mn_{1/3})C_2O_4{\cdot}2H_2O$ was prepared. The oxide powders of $(Ni_{1/3}Co_{1/3}Mn_{1/3})_3O_4$ can be obtained by thermally decomposing the oxalate under air atmosphere. Therefore, the transition metals in the spent LIBs can be recovered in the forms of metals or oxides by the oxalic acid leaching–thermal decomposition process. And then, the recovered metals or oxides are potential microwave absorbers.

The morphologies and structures of powders have important influences on their microwave absorbing properties. It has been proved that porous structures and fibrous morphologies are beneficial to enhanced microwave absorbing properties [41, 42]. In the past years, many Co-based microwave absorbing materials were studied due to their excellent magnetic properties. However, the porous Co fibers have rarely been reported. The porous structure can be obtained by thermal decomposition of cobalt oxalate due to the release of CO_2 gas in the decomposition process. The fibrous morphology can be inherited from rod-like cobalt oxalate precursors. However, in all of the above oxalic acid leaching processes, the morphologies of the oxalate powders were not researched systematically, and the powders are irregular and aggregate particles. In the work of Park et al. [43], rod-like cobalt oxalate powders were obtained from the cathode materials by using malic acid as a leaching agent and oxalic acid as a precipitant. However, these cobalt oxalate rods are not uniform and slightly agglomerated. The uneven particles in absorbing matrix will lead to deteriorating microwave absorbing performance. In addition, in order to obtain one dimensional powder, some templates such as carbon nanotubes [44] and anodic aluminum oxide [45] were usually employed, which make the preparation be very complicated. Therefore, it is still a challenge to directly obtain uniform and dispersive cobalt oxalate rods from the cathode materials by oxalic acid leaching-precipitation process. In this paper, we developed a simple template-free method to prepare long rod-like $CoC_2O_4{\cdot}2H_2O$ powders using oxalic acid to leach the $LiCoO_2$ cathode materials, just by choosing a leaching condition with suitable leaching temperature. The porous Co microfibers were obtained by thermal decomposition of the $CoC_2O_4{\cdot}2H_2O$ rods and they showed excellent microwave absorbing properties in 2–18 GHz.

2 Experimental

2.1 Pretreatment of spent LIBs

Spent LIBs with $LiCoO_2$ cathodes used in this study were purchased from a local recycling center. These spent LIBs were firstly discharged in a 10 wt% NaCl solution for 48 h and then manually dismantled into plastic cases, cathodes, anodes and organic separators. The cathode active powders were separated from aluminum foils by immersing the cathodes in N-methyl-2-pyrrolidone (NMP) at 80 °C for 2 h. After filtering and washing, the cathode active powders were dried at 60 °C for the subsequent process.

2.2 Preparation of porous Co microfibers

Oxalic acid was used to treat the collected cathode active powders. In a typical process, 0.5 g cathode powders were added into 50 ml $H_2C_2O_4$ solution (1 $mol{\cdot}L^{-1}$) under stirring. The detailed leaching conditions (S1–S6) are shown in Table 1. After stirred for 2 h, the black cathode

Table 1 Operation conditions of oxalic acid leaching process

Sample number	Temperature / °C	Time / h
S1	50	2
S2	60	2
S3	70	2
S4	80	2
S5	50 °C for 1 h and then 80 °C for 1 h	
S6	60 °C for 1 h and then 80 °C for 1 h	

powders were converted to pink oxalate precipitates. After filtering, washing and drying, the oxalate powders were calcined under 420 °C for 30 min in nitrogen, and then the porous Co microfibers can be obtained by magnetic separation from the decomposed products.

2.3 Materials characterization

The cathode powders were dissolved in aqua regia solution to determine the chemical composition. The compositions of both the aqua regia and leaching solution were determined by an inductively coupled plasma optical emission spectrometer (ICP-OES, ICPS-7510 PLUS, Shimadzu, Japan). Crystal structures of the samples were characterized by an X-ray diffractometer (XRD, D8 Advance, Bruker, Germany), and the morphologies of the samples were determined by a scanning electron microscope (SEM, JSM-6490LV, JEOL, Japan) and a transmission electron microscope (TEM, JEM-2100, JEOL, Japan). Thermal decomposition process of the oxalate powders was determined by a thermogravimetric–differential thermal analyzer (TG-DTA, DTG-60H, Shimadzu, Japan) with a scanning speed of 10 °C·min^{-1} from room temperature to 500 °C under nitrogen. For the microwave absorption measurement, the Co microfibers were first mixed with 75 wt% paraffin homogeneously and then shaped into a concentric ring with 7.00 mm in outer diameter and 3.04 mm in inner diameter. EM parameters of the concentric ring were characterized using a vector network analyzer (Agilent E5071C) in the frequency of 2–18 GHz. Reflection loss (RL) of the sample was calculated according to the transmission line theory based on the measured EM parameters.

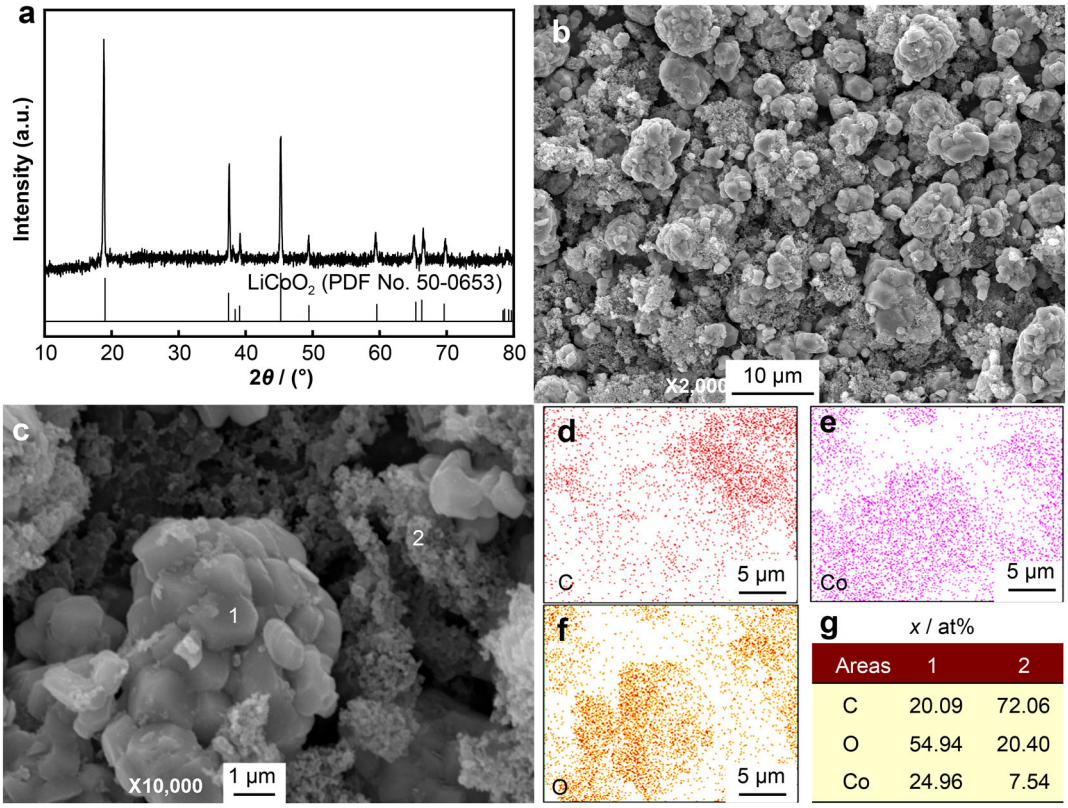

Fig. 1 **a** XRD pattern and **b, c** SEM images of cathode powders; **d–f** EDS mapping and **g** EDS composition of powders in **c**

3 Results and discussion

3.1 Oxalic acid leaching of cathode powders

Crystal structure, morphology and composition of the cathode powders were determined by XRD, SEM images and EDS, as shown in Fig. 1. It is seen from Fig. 1a that the main phase of the cathode powders is $LiCoO_2$ (PDF No. 50-0653). However, two different powders exist in the SEM images (Fig. 1b, c). According to EDS mapping and the compositions of Areas 1 and 2 shown in Fig. 1d–g, the coarse particles in Fig. 1c are $LiCoO_2$ and the fine powders are carbon black. The carbon black is amorphous, so there is no obvious carbon characteristic peak in the XRD pattern.

It is well known that trivalent Co in $LiCoO_2$ is difficult to be leached out. However, in the oxalic acid leaching process, the trivalent Co can be reduced to divalent Co due to the reducibility of oxalic acid. Figure 2a shows the Li^+ leaching rate and Co^{2+} concentration in the leaching solution at different leaching parameters. It can be seen that the leaching rate of Li^+ is proportional to the leaching temperature, while the Co^{2+} concentration shows a contrary trend. It has been proved by plenty of literatures that the leaching rates of cathode materials can be improved by increasing the leaching temperature [21, 46–48]. Therefore, the Li^+ leaching rate increases from 44.33% to 91.01% when the leaching temperature increases from 50 to 80 °C. With the increased temperature, the Co^{2+} leaching rate should also increase. However, the Co^{2+} concentrations at high temperatures are decreased, which indicates that the Co^{2+} precipitation rate also increases proportionately to the reaction temperature, and more Co^{2+} can be converted to oxalate precipitates at a higher temperature.

XRD patterns of the leaching residues under different leaching conditions are shown in Fig. 2b. It is observed that both $LiCoO_2$ (PDF No. 50-0653) and $CoC_2O_4{\cdot}2H_2O$ (PDF No. 25-0250) exist in S1 and S2, indicating low leaching rates. Conversely, for S3 and S4, the characteristic peaks of $LiCoO_2$ are almost disappeared due to the high leaching rates at high leaching temperatures. Therefore, the leaching process can be described as follows:

$$2LiCoO_2(s) + 4H_2C_2O_4 = Li_2C_2O_4 + 2CoC_2O_4{\cdot}2H_2O(s) + 2H_2O + 2CO_2 \quad (1)$$

It should be pointed out that there is an obvious difference for the peak intensity of (400) crystal face (2θ = 30.07°) between the $CoC_2O_4{\cdot}2H_2O$ sample and the standard card. This may be due to the preferred orientation growth of $CoC_2O_4{\cdot}2H_2O$ crystals, which will be proved by the following SEM images.

Figure 3 shows SEM images of the leaching residues under different leaching conditions. Both unreacted $LiCoO_2$ particles and newly generated $CoC_2O_4{\cdot}2H_2O$ particles exist in the residues. At low leaching temperatures (50 and 60 °C), the $CoC_2O_4{\cdot}2H_2O$ particles are long rod-like. At the leaching temperature of 70 °C, the $CoC_2O_4{\cdot}2H_2O$ particles show polyhedral shapes and the polyhedral particles are agglomerated. When the leaching temperature increases to 80 °C, the agglomeration of the particles is more severe. This phenomenon indicates that the growth of the $CoC_2O_4{\cdot}2H_2O$ is closely related to the reaction temperature. It is well known that the morphologies of particles are controlled by the nucleation and growth of the crystals. At low temperatures, the growth speed of crystals is slow, which is beneficial to the oriented growth of the crystals. Conversely, at high temperatures, the leaching speed is fast, and the nucleation and growth are quick, which lead to the formation of the agglomerated particles. It also can be found in Fig. 3 that the unreacted $LiCoO_2$ particles are decreased with the increased temperature, due to the increased leaching rate shown in Fig. 2a.

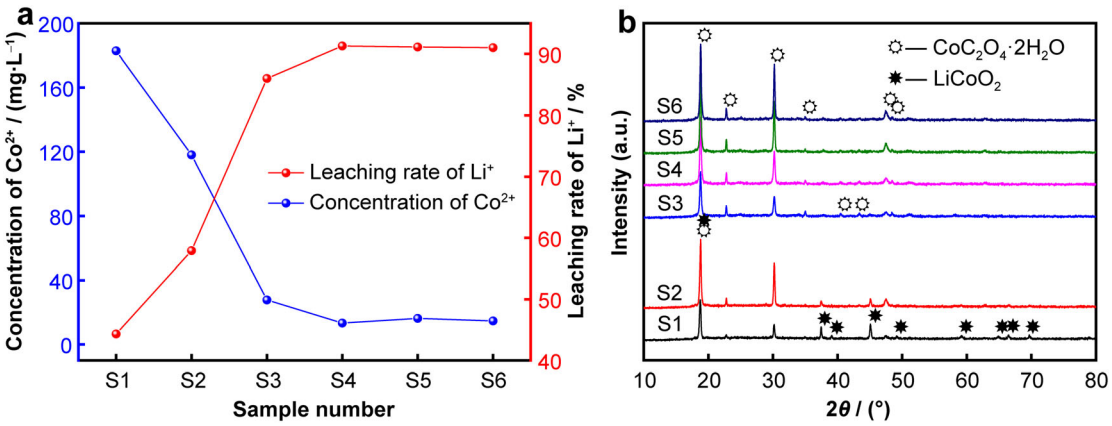

Fig. 2 **a** Leaching rate of Li^+ and concentration of Co^{2+} in leaching solution; **b** XRD patterns of leaching residues of S1–S6

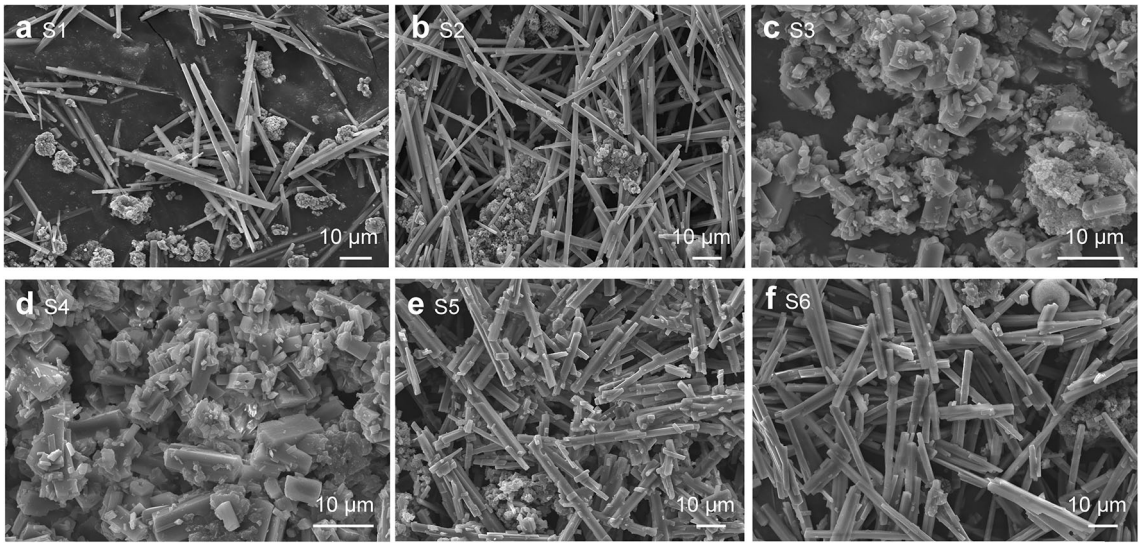

Fig. 3 SEM images of leaching residues of **a** S1, **b** S2, **c** S3, **d** S4, **e** S5 and **f** S6

It seems impossible to obtain a high leaching rate and rod-like $CoC_2O_4{\cdot}2H_2O$ particles simultaneously from the above analysis. In order to solve this contradictory, two additional two-stage leaching experiments (S5 and S6) were carried out. It is seen from Fig. 2a that the leaching rates of S5 and S6 are roughly identical to that of S4. However, the $CoC_2O_4{\cdot}2H_2O$ morphologies of S5 and S6 shown in Fig. 3e, f are similar to those of S1 and S2. In the two-stage leaching process, the rod-like $CoC_2O_4{\cdot}2H_2O$ particles were first produced at lower temperatures. And then new Co^{2+} leached in the second stage will combine $C_2O_4^{2-}$ and continue to grow on the surfaces of the formed $CoC_2O_4{\cdot}2H_2O$ rods. Therefore, the diameters of the rods of S5 and S6 are slightly larger than those of S1 and S2. By comparing Fig. 3e, f, it is shown that S6 has a better rod-like morphology than S5, which can be ascribed to that more Co^{2+} are leached out for S5 in the second stage. The supersaturation of Co^{2+} will lead to the generation of some new fine particles. As is clear from the above descriptions, the high leaching rate and rod-like $CoC_2O_4{\cdot}2H_2O$ particles can be obtained simultaneously just by choosing a leaching condition with suitable temperatures.

3.2 Preparation of porous Co microfibers

Thermal decomposition behavior of the leaching residues (S6) in N_2 atmosphere was characterized by TG-DSC analysis, as shown in Fig. 4a. It can be seen that there are two obvious weight loss stages in the TG curve, which is consistent with some other reported thermal decomposition of oxalate powders [21, 40]. The first weight loss of 18.04% is corresponding to the dehydration of $CoC_2O_4{\cdot}2H_2O$ powders, and the second weight loss of 46.01% can be ascribed to the decomposition of CoC_2O_4 powders (Fig. 4b). It is noted that both the two theoretical weight losses are slightly larger than the practical weight losses. This is because there are a small number of carbon black and unreacted $LiCoO_2$ in the residues, which are stable in the N_2 atmosphere. It is also found in Fig. 4a that there are two endothermic peaks at 193 and 388 °C in the DSC curve, corresponding to the two weight loss stages in the TG curve, which indicates that both of the two weight loss stages are endothermic processes.

Figure 4c shows XRD pattern of the obtained Co powders through thermal decomposition process. It is shown that there are two Co crystal forms in the powders, corresponding to the hexagonal structure (PDF No. 05-0727) and face-centered cubic structure (PDF No. 15-0806), respectively. Figure 4d is SEM image of the Co powders, showing that the Co powders have fibrous shapes with diameters of 1–2 μm. This fibrous shape helps to get an improved magnetic property because of its obvious shape anisotropy, and then lead to enhanced microwave absorption [42]. Owing to the release of H_2O and CO_2 in the thermal decomposition process, the microfibers show porous structures, and each microfiber consists of small particles with size of 100–200 nm (the magnified SEM image is shown in Fig. S1). Porous structure and composition of the Co fibers were further determined by TEM image (Fig. 4e) and corresponding EDS mapping (Fig. 4f and Fig. S2). These pores in the fibers can cause multiple reflection and scattering of the incident EM waves, and thus enhance the microwave absorbing property.

3.3 Electromagnetic parameters

The microwave absorption performance of a material depends on its electromagnetic parameters (relative

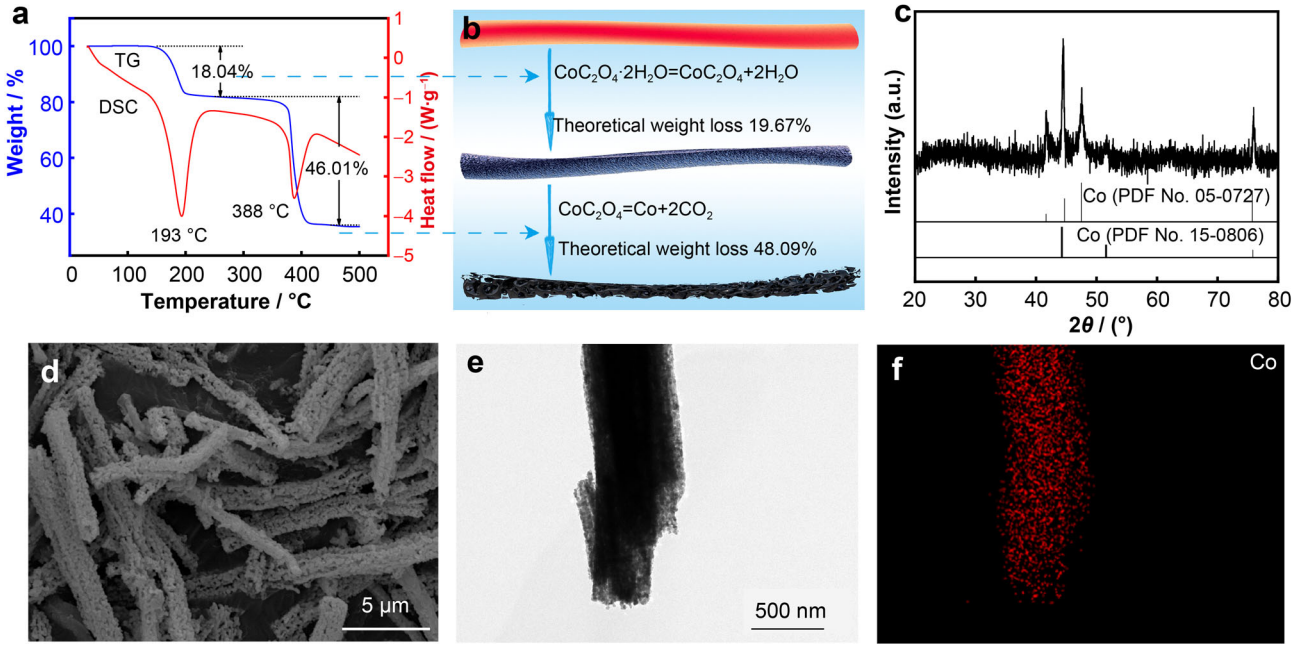

Fig. 4 **a** TG-DSC curves and **b** decomposition mechanism of $CoC_2O_4{\cdot}2H_2O$ powders; **c** XRD pattern, **d** SEM image, **e** TEM image and **f** EDS mapping of Co fibers

complex permittivity of $\varepsilon_r = \varepsilon' - j\varepsilon''$, and relative complex permeability of $\mu_r = \mu' - j\mu''$, where ε' and ε'' are real and imaginary parts of the permittivity, and μ' and μ'' are real and imaginary parts of the permeability, respectively [49]. Figure 5a presents the permittivity of Co/paraffin composite. It is shown that both ε' and ε'' fluctuate in the whole 2–18 GHz. As is well known, the dielectric polarization mechanism can be from interfacial polarization, dipolar polarization, ionic polarization and electronic polarization. Generally, the latter two mainly happen in infrared and ultraviolet frequency bands, respectively, and the interfacial polarization only appears in low-frequency band less than 100 Hz. It is interesting from Fig. 5a to find that each resonance peak in the ε'' curve corresponds to a descent stage of ε' marked with green background, which is the typical characteristic of dipolar polarization. The Debye Function was usually employed to describe the dipolar polarization as shown in Eq. (2) [50]:

$$\varepsilon(f) = \varepsilon_\infty + \frac{\varepsilon_s - \varepsilon_\infty}{1 + j2\pi f\tau} = \varepsilon'(f) + j\varepsilon''(f) \quad (2)$$

where ε_s, ε_∞ and τ are the static permittivity, optical permittivity at the high-frequency limit, and relaxation time, respectively; and f is frequency. Equation (2) indicates that the plot of ε' versus ε'' should be a semicircle, i.e., the Cole–Cole semicircle [51]. It is shown in Fig. 5c that four semicircles were obtained by plotting the ε'-ε'' curves, and they exactly match up with the green parts shown in Fig. 5a. Therefore, it can be concluded that the dipolar polarization should be the main polarization mechanism of the Co/paraffin composite.

Figure 5b presents the permeability of Co/paraffin composite. It is shown that the μ' first exhibits a sharp decline from 2.26 to 0.94 in 2.00–7.76 GHz, and then a slow ascent in 7.76–18.00 GHz. Correspondingly, the μ'' curve presents three resonance peaks at about 4.08, 5.36 and 12.56 GHz. Generally, the magnetic loss mechanism can be ascribed to magnetic hysteresis loss, domain-wall resonance, eddy current loss and natural resonance. In weak fields, the magnetic hysteresis loss disappears due to the reversible magnetic process. The domain-wall resonance mainly happens in 1–100 MHz. Therefore, the first two losses are negligible in this study. If the eddy current loss is predominant, the value of $\mu''(\mu')^{-2}f^{-1}$ should keep unchanged with the varied frequencies. However, Fig. 5d shows that there is a drastic change for the $\mu''(\mu')^{-2}f^{-1}$ curve in 2–18 GHz. Therefore, the magnetic loss is primarily from natural resonance.

The real parts of the electromagnetic parameters reflect energy storage and the imaginary parts reflect energy dissipation. Therefore, the dielectric loss factor ($\tan\delta_e = \varepsilon''/\varepsilon'$) and magnetic loss factor ($\tan\delta_m = \mu''/\mu'$) can be used as the representation of electromagnetic loss capacities. As shown in Fig. S3, $\tan\delta_m$ is larger than $\tan\delta_e$ at all frequencies, which means the predominance of magnetic loss for the Co/paraffin composite. This is a common phenomenon for the magnetic absorbing materials [34, 41, 42].

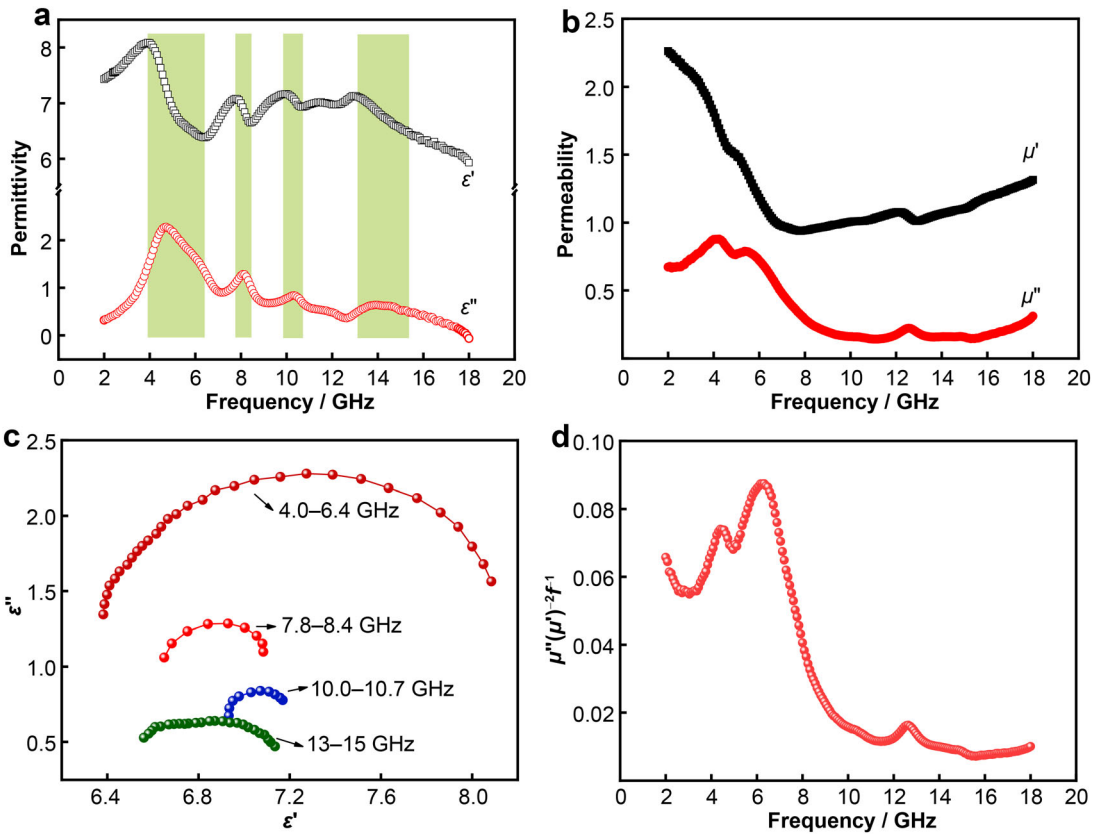

Fig. 5 **a** Complex permittivity, **b** complex permeability, **c** Cole–Cole semicircle and **d** value of $\mu''(\mu')^{-2}f^{-1}$ of Co/paraffin composite

3.4 Microwave absorbing properties

The reflection loss (RL) is the most commonly used indicator to reflect the microwave absorbing property. According to the transmission line theory, the RL can be calculated by Eqs. (3, 4):

$$Z_{\text{in}} = \sqrt{\frac{\mu_{\text{r}}}{\varepsilon_{\text{r}}}}\tanh\left(j\frac{2\pi f}{c}d\sqrt{\varepsilon_{\text{r}}\mu_{\text{r}}}\right) \tag{3}$$

$$\text{RL} = 20\lg\left|\frac{Z_{\text{in}} - 1}{Z_{\text{in}} + 1}\right| \tag{4}$$

where Z_{in} is the normalized input impedance, μ_{r} is relative complex permeability, ε_{r} is relative complex permittivity, c is the light velocity in free space (3×10^8 m·s^{-1}), f is electromagnetic wave frequency (Hz) and d is the sample thickness (m).

RL of the Co/paraffin sample at different conditions were calculated and the results are shown in Fig. 6a, b. It is shown that at the sample thickness of 4.5 mm, the minimum RL reach − 36.14 and − 38.20 dB at 4.16 and 17.60 GHz, respectively. The relationship between RL and electromagnetic wave absorptivity (η) can be described by Eq. (5):

$$\text{RL} = 10\lg(1 - \eta) \tag{5}$$

which shows that only less than 10% of the introduced electromagnetic wave is reflected when the RL value is lower than − 10 dB. And so, the bandwidth of RL less than − 10 dB is often defined as effective bandwidth. For the Co/paraffin composite with a thickness of 4.5 mm, the frequency ranges of RL < − 10 dB are 3.36–7.44 GHz and 16.56–18.0 GHz. The effective bandwidth reaches up to 5.52 GHz.

It is also found from Fig. 6a, b that the peak frequencies of RL move toward lower frequencies when the sample thickness is increased. In addition, when the thickness increases to 4.5 mm, two minimum RL appear at different frequencies. The relationship between the peak frequency (f_{m}) and the corresponding matching thickness (t_{m}) can be described by the quarter-wavelength model as shown in Eq. (6) [52], where c is the light velocity in free space, 3×10^8 m·s^{-1}:

$$t_{\text{m}} = \frac{nc}{4f_{\text{m}}\sqrt{|\mu_{\text{r}}||\varepsilon_{\text{r}}|}} \quad (n = 1, 3, 5, \ldots) \tag{6}$$

Which indicates that t_{m} is in inverse ratio to f_{m}, and a t_{m} may match more than one f_{m} due to the variable n. Figure 6c is the calculated results according to Eq. (6), and Fig. 6d is the projection map of Fig. 6b. Taking the 4.5 mm sample for example, it shows that the peak

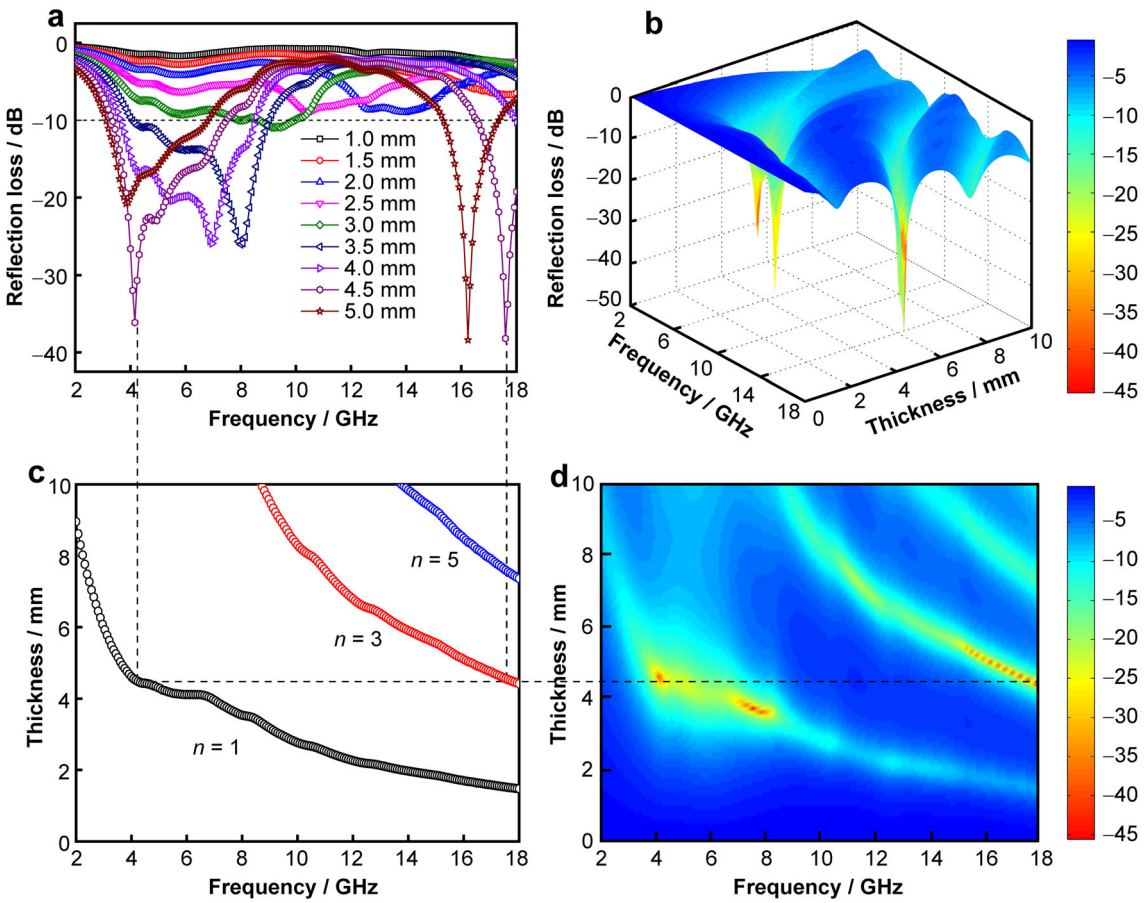

Fig. 6 **a** Two-dimensional and **b** three-dimensional graphs of reflection loss; **c** simulated curves according to Eq. (6) and **d** three-dimensional projection of Co/paraffin sample

frequencies in Fig. 6a, d agree well with the simulated results in Fig. 6c, which confirms the quarter-wavelength absorption mechanism.

3.5 Environmental evaluation

With the development of industry, environmental pollution has become a severe global problem. In the past few years, it has attracted wide concern to recycle the valuable metals from spent LIBs, and eliminate the potential harm of the hazardous materials in spent LIBs. In addition, electromagnetic radiation has become a new pollutant source with the extensive use of wireless communication and electronic devices. In this research, we developed a novel process to prepare porous Co microfibers from spent LIBs for efficient microwave absorption. Therefore, this work is helpful to reduce the hazards of spent LIBs and electromagnetic radiation to environment and human health simultaneously.

Below are some environmental advantages based on this research. Firstly, compared with the strong inorganic acids (H_2SO_4, HCl and HNO_3) leaching, oxalic acid leaching is relatively moderate, and its negative influence on equipment and discharged waste water is decreased. Considering the possible environmental toxicity of oxalate ions, two potential approaches were proposed for the recycling of oxalate ions (Fig. S4). In addition, the lithium and cobalt can be separated in one step due to the solubility difference of their oxalates, which avoids the complicated separation processes in the inorganic acid leaching. Secondly, the lithium in the leaching solution is suited to be recycled in the form of Li_2CO_3 easily. Up to now, many studies on the recycling of Li_2CO_3 have been reported [53, 54], therefore, Li recovery from its carbonate salt was not investigated in this work. Thirdly, multiple factors including the porous structures, fibrous morphologies, dipolar polarization, natural resonance and the quarter-wavelength absorption mechanism contributed to the excellent microwave absorbing property, as shown in Fig. 7. Therefore, the porous Co microfibers exhibit an enhanced microwave absorbing property compared with some other Co-based materials, as shown in Fig. 8 [55–62]. This means that the Co microfibers can be made into a potential microwave absorbing coating to absorb radar waves for the military stealth, or protect precision

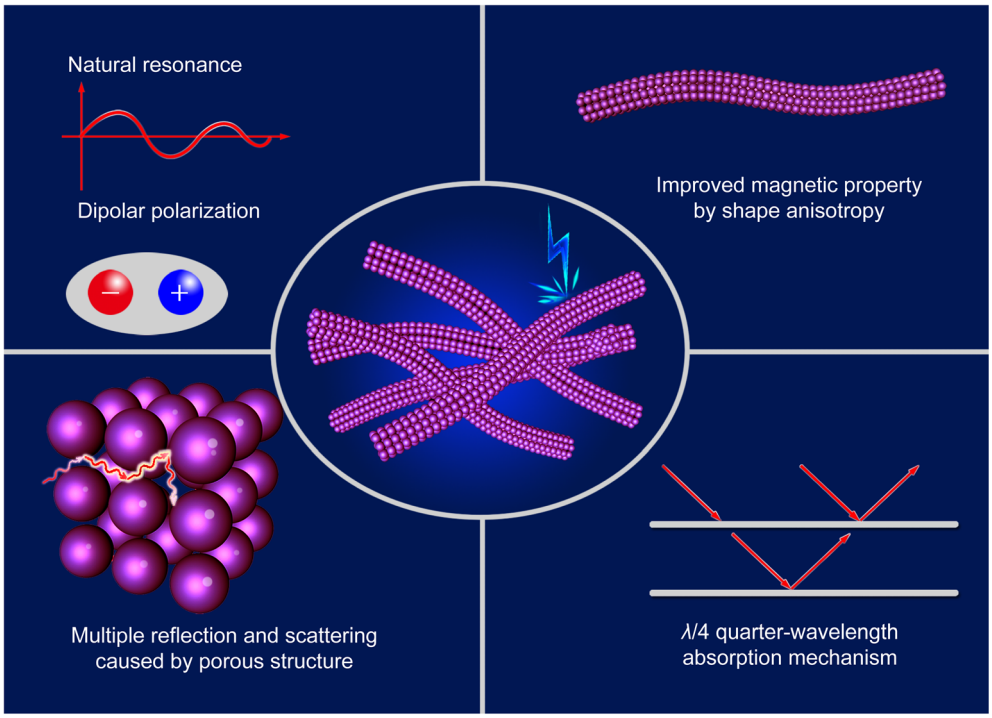

Fig. 7 Microwave absorbing mechanism of porous Co microfibers

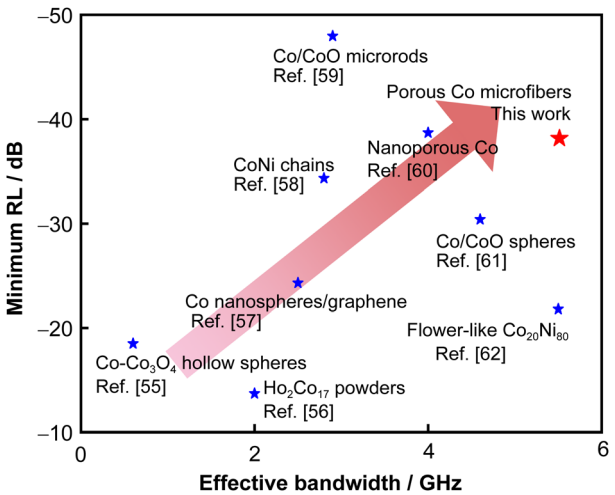

Fig. 8 Microwave absorbing properties of different Co-based materials

equipment and people from the electromagnetic interference and radiation.

4 Conclusion

In conclusion, the porous Co microfibers were prepared using spent LIBs as raw materials through a template-free method. Firstly, a high leaching rate and rod-like $CoC_2O_4{\cdot}2H_2O$ particles were obtained simultaneously through oxalic acid leaching at a suitable temperature. Secondly, the porous Co microfibers were prepared by thermally decomposing the cobalt oxalate powders under 420 °C for 30 min in nitrogen. The prepared Co microfibers (25 wt%)/paraffin sample exhibited an excellent microwave absorbing property. The dielectric loss and magnetic loss of the sample mainly come from dipolar polarization and natural resonance, respectively, and the magnetic loss is predominant. At the sample thickness of 4.5 mm, the RL reach − 36.14 and − 38.20 dB at 4.16 and 17.60 GHz, respectively, and the effective bandwidth is up to 5.52 GHz. This indicates that the porous Co microfiber is a promising candidate for strong and broadband microwave absorption. Therefore, this study provides a new method to make high value-added products from the spent LIBs.

Acknowledgements This study was financially supported by the National Natural Science Foundation of China (Nos. 51604005 and U1703130), the Universities Natural Science Research Project of Education Department of Anhui Province (No. KJ2020A0224), and the Open Fund of Anhui Province Key Laboratory of Metallurgical Engineering & Resources Recycling (No. SKF19-01).

Declarations

Conflict of interests The authors declare that they have no conflict of interest.

References

[1] Hu J, Zhang J, Li H, Chen Y, Wang C. A promising approach for the recovery of high value-added metals from spent lithium-ion batteries. J Power Sour. 2017;351:192.

[2] Xiao WL, Zheng YJ, He HB. Cascade extraction of lithium in anode of waste lithium ion battery. Chin J Rare Met. 2020; 44(10):1078.

[3] Lv WG, Wang ZH, Cao HB, Sun Y, Zhang Y, Sun Z. A critical review and analysis on the recycling of spent lithium-ion batteries. ACS Sustain Chem Eng. 2018;6(2):1504.

[4] Yao Y, Zhu M, Zhao Z, Tong B, Fan Y, Hua Z. Hydrometallurgical processes for recycling spent lithium-ion batteries: a critical review. ACS Sustain Chem Eng. 2018;6(11):13611.

[5] Yao Y, Zhu M, Zhao Z, Liu W, Tong B, Li M. Density functional theory study of selectivity of crown ethers to Li^+ in spent lithium-ion batteries leaching solutions. Chin J Chem Phys. 2019;32(3):343.

[6] Liu C, Qiu XY, Liu Y, He XJ, Chen ZQ, Liu MD. Research status and prospects of physical separation technology of spent lithium-ion batteries. Chin J Rare Met. 2021;45(4):493.

[7] Sun Y, Zhu MY, Yao YL, Wang HW, Tong BH, Zhao Z. A novel approach for the selective extraction of Li^+ from the leaching solution of spent lithium-ion batteries using benzo-15-crown-5 ether as extractant. Sep Purif Technol. 2020;237: 116325.

[8] Mrozik W, Rajaeifar MA, Heidrich O, Christensen P. Environmental impacts, pollution sources and pathways of spent lithium-ion batteries. Energy Environ Sci. 2021;14(12):6099.

[9] Chen XP, Guo CX, Ma HR, Li JZ, Zhou T, Cao L, Kang DZ. Organic reductants based leaching: a sustainable process for the recovery of valuable metals from spent lithium ion batteries. Waste Manag. 2018;75:459.

[10] Meng Q, Zhang YJ, Dong P. Use of electrochemical cathode-reduction method for leaching of cobalt from spent lithium-ion batteries. J Clean Prod. 2018;180:64.

[11] Wang M, Tan Q, Li J. Unveiling the role and mechanism of mechanochemical activation on lithium cobalt oxide powders from spent lithium-ion batteries. Environ Sci Technol. 2018; 52(22):13136.

[12] Gao W, Zhang X, Zheng X, Lin X, Cao H, Zhang Y, Sun Z. Lithium carbonate recovery from cathode scrap of spent lithium-ion battery: a closed-loop process. Environ Sci Technol. 2017;51(3):1662.

[13] Zhang J, Hu J, Zhang W, Chen Y, Wang C. Efficient and economical recovery of lithium, cobalt, nickel, manganese from cathode scrap of spent lithium-ion batteries. J Clean Prod. 2018; 204:437.

[14] Li SN, Luo SH, Yang L, Wang Q, Zhang YH, Liu X. Synthesis and electrochemical properties of $LiFePO_4$ cathode material by ionic thermal method using eutectic mixture of tetramethyl ammonium chloride-urea. Real Met. 2021;40(12):3477.

[15] Zhang JL, Hu JT, Liu YB, Jing QK, Yang C, Chen YQ, Wang CY. Sustainable and facile method for the selective recovery of lithium from cathode scrap of spent $LiFePO_4$ batteries. ACS Sustain Chem Eng. 2019;7(6):5626.

[16] Mahandra H, Ghahreman A. A sustainable process for selective recovery of lithium as lithium phosphate from spent $LiFePO_4$ batteries. Resour Conserv Recycl. 2021;175:105883.

[17] Xiao J, Li J, Xu Z. Novel approach for in situ recovery of lithium carbonate from spent lithium ion batteries using vacuum metallurgy. Environ Sci Technol. 2017;51(20):11960.

[18] Yi AF, Zhu ZW, Liu YH, Zhang J, Su H, Qi T. Using highly concentrated chloride solutions to leach valuable metals from cathode-active materials in spent lithium-ion batteries. Rare Met. 2021;40(7):1971.

[19] Hanada T, Seo K, Yoshida W, Fajar ATN, Goto M. DFT-based investigation of amic-acid extractants and their application to the recovery of Ni and Co from spent automotive lithium-ion batteries. Sep Purif Technol. 2022;281:119898.

[20] Jiang Y, Chen X, Yan S, Li S, Zhou T. Pursuing green and efficient process towards recycling of different metals from spent lithium-ion batteries through Ferro-chemistry. Chem Eng J. 2021;426:131637.

[21] Sun L, Qiu KQ. Organic oxalate as leachant and precipitant for the recovery of valuable metals from spent lithium-ion batteries. Waste Manag. 2012;32(8):1575.

[22] Chen X, Kang D, Li J, Zhou T, Ma H. Gradient and facile extraction of valuable metals from spent lithium ion batteries for new cathode materials re-fabrication. J Hazard Mater. 2020;389: 121887.

[23] He LP, Sun SY, Yu JG. Performance of $LiNi_{1/3}Co_{1/3}Mn_{1/3}O_2$ prepared from spent lithium-ion batteries by a carbonate co-precipitation method. Ceram Int. 2018;44(1):351.

[24] Sandhya CP, John B, Gouri C. Synthesis, characterization and electrochemical evaluation of mixed oxides of nickel and cobalt from spent lithium-ion cells. RSC Adv. 2016;6(115): 114192.

[25] Yao L, Yao HS, Xi GX, Feng Y. Recycling and synthesis of $LiNi_{1/3}Co_{1/3}Mn_{1/3}O_2$ from waste lithium ion batteries using D, L-malic acid. RSC Adv. 2016;6(22):17947.

[26] Yu J, Liu Y, Han S, Tan Q, Liu L, Li J. Unveiling sodium ion pollution in spray-dried precursors and its implications for the green upcycling of spent lithium-ion batteries. Environ Sci Technol. 2021;55(21):14897.

[27] Li X, Guo X, Liu T, Zheng X, Bai J. Shape-controlled synthesis of Fe nanostructures and their enhanced microwave absorption properties at L-band. Mater Res Bull. 2014;59:137.

[28] Liu W, Shao QW, Ji GB, Liang XH, Cheng Y, Quan B, Du YW. Metal-organic-frameworks derived porous carbon-wrapped Ni composites with optimized impedance matching as excellent lightweight electromagnetic wave absorber. Chem Eng J. 2017; 313:734.

[29] Zhang C, Yao Y, Zhan J, Wu J, Li C. Template-free synthesis of Ni microfibres and their electromagnetic wave absorbing properties. J Phys D: Appl Phys. 2013;46(49):495308.

[30] Liu Q, Zhang D, Fan T. Electromagnetic wave absorption properties of porous carbon/Co nanocomposites. Appl Phys Lett. 2008;93(1):013110.

[31] Wu XM, Yao YL, Fan YQ, Zhao Z, Zhan J. Designing Co-based microwave absorber with high absorption and thin thickness based on structure regulations. J Mater Sci: Mater Electron. 2021;32(24):28648.

[32] Ma JR, Wang XX, Cao WQ, Han C, Yang HJ, Yuan J, Cao MS. A facile fabrication and highly tunable microwave absorption of 3D flower-like Co_3O_4-rGO hybrid-architectures. Chem Eng J. 2018;339:487.

[33] Feng J, Zong Y, Sun Y, Zhang Y, Yang X, Long GK, Wang Y, Li XH, Zheng XL. Optimization of porous $FeNi_3$/N-GN composites with superior microwave absorption performance. Chem Eng J. 2018;345:441.

[34] Yao Y, Zhu M, Zhang C, Fan Y, Zhan J. Effects of composition on the microwave absorbing properties of Fe_xNi_{100-x} (x = 0–25) submicro fibers. Adv Powder Technol. 2018;29(5):1099.

[35] Jiang Q, Li H, Cao Z, Li H, Wang Q, Jiang Z, Kuang Q, Xie Z. Synthesis and enhanced electromagnetic wave absorption performance of amorphous Co_xFe_{10-x} alloys. J Alloys Compd. 2017; 726:1255.

[36] Park JH, Ro JC, Suh SJ. Fe/Co ratio dependent excellent microwave absorption of FeCo alloys with a wide bandwidth in the high-frequency region. Mater Res Bull. 2022;145:111513.
[37] Liu X, Wu N, Cui C, Bi N, Sun Y. One pot synthesis of Fe_3O_4/MnO_2 core-shell structured nanocomposites and their application as microwave absorbers. RSC Adv. 2015;5(31):24016.
[38] Zhan J, Yao Y, Zhang C, Li C. Synthesis and microwave absorbing properties of quasione-dimensional mesoporous $NiCo_2O_4$ nanostructure. J Alloys Compd. 2014;585:240.
[39] Zeng XL, Li JH, Shen BY. Novel approach to recover cobalt and lithium from spent lithium-ion battery using oxalic acid. J Hazard Mater. 2015;295:112.
[40] Zhang XX, Bian YF, Xu SWY, Fan ES, Xue Q, Guan YBA, Wu F, Li L, Chen RJ. Innovative application of acid leaching to regenerate $Li(Ni_{1/3}Co_{1/3}Mn_{1/3})O_2$ cathodes from spent lithium-ion batteries. ACS Sustain Chem Eng. 2018;6(5):5959.
[41] Yao Y, Zhang C, Fan Y, Zhan J. Preparation and microwave absorbing property of porous FeNi powders. Adv Powder Technol. 2016;27(5):2285.
[42] Yao Y, Zhang C, Fan Y, Zhan J. Preparation of $Fe_{20}Ni_{80}$ submicron fibers by an oxalate precipitation-thermal decomposition process and their microwave absorbing properties. J Mater Sci: Mater Electron. 2017;28(18):13548.
[43] Park YM, Lim H, Moon JH, Lee HN, Son SH, Kim H, Kim HJ. High-yield one-pot recovery and characterization of nanostructured cobalt oxalate from spent lithium-ion batteries and successive re-synthesis of $LiCoO_2$. Metals. 2017;7(8):303.
[44] Lv R, Kang F, Cai D, Wang C, Gu J, Wang K, Wu D. Long continuous FeNi nanowires inside carbon nanotubes: synthesis, property and application. J Phys Chem Solids. 2008;69(5–6):1213.
[45] Atalay FE, Kaya H, Atalay S, Tari S. Influences of deposition time and pH on magnetic NiFe nanowires fabrication. J Alloys Compd. 2009;469(1–2):458.
[46] Li L, Bian YF, Zhang XX, Guan YB, Fan ES, Wu F, Chen RJ. Process for recycling mixed-cathode materials from spent lithium-ion batteries and kinetics of leaching. Waste Manag. 2018;71:362.
[47] Li L, Bian YF, Zhang XX, Xue Q, Fan ES, Wu F, Chen RJ. Economical recycling process for spent lithium-ion batteries and macro- and micro-scale mechanistic study. J Power Sour. 2018;377:70.
[48] Sun CH, Xu LP, Chen XP, Qiu TY, Zhou T. Sustainable recovery of valuable metals from spent lithium-ion batteries using DL-malic acid: leaching and kinetics aspect. Waste Manag Res. 2018;36(2):113.
[49] Wang P, Liu PA, Ye S. Preparation and microwave absorption properties of Ni(Co/Zn/Cu)Fe_2O_4/SiC@SiO_2 composites. Rare Met. 2019;38(1):59.
[50] Zhang X, Rao Y, Guo J, Qin G. Multiple-phase carbon-coated $FeSn_2$/Sn nanocomposites for high-frequency microwave absorption. Carbon. 2016;96:972.
[51] Xie Z, Geng D, Liu X, Ma S, Zhang Z. Magnetic and microwave-absorption properties of graphite-coated (Fe, Ni) nanocapsules. J Mater Sci Technol. 2011;27(7):607.
[52] Wei J, Zhang Z, Wang B, Wang T, Li F. Microwave reflection characteristics of surface-modified $Fe_{50}Ni_{50}$ fine particle composites. J Appl Phys. 2010;108(12):123908.
[53] Meshram P, Pandey BD, Mankhand TR. Hydrometallurgical processing of spent lithium ion batteries (LIBs) in the presence of a reducing agent with emphasis on kinetics of leaching. Chem Eng J. 2015;281:418.
[54] Zhu SG, He WZ, Li GM, Zhou X, Zhang XJ, Huang JW. Recovery of Co and Li from spent lithium-ion batteries by combination method of acid leaching and chemical precipitation. Trans Nonferrous Met Soc China. 2012;22(9):2274.
[55] Wu H, Wu Q, Wang L. Design and wide range microwave absorption of porous Co–Co_3O_4 hybrid hollow sphere with magnetic multi-resonance mechanisms. Mater Charact. 2015;103:1.
[56] He C, Pan S, Cheng L, Liu X, Wu Y. Effect of rare earths on microwave absorbing properties of RE-Co alloys. J Rare Earths. 2015;33(3):271.
[57] Yan FF, Zong Y, Zhao CJ, Tan GG, Sun Y, Li XH, Ren ZY, Zheng XL. Porous Co nanospheres supported on nitrogen-doped graphene as high-efficiency electromagnetic wave absorbers with thin thickness. J Alloys Compd. 2018;742:928.
[58] Zhao B, Shao G, Fan B, Xie Y, Zhang R. Preparation and electromagnetic wave absorption of chain-like CoNi by a hydrothermal route. J Magn Magn Mater. 2014;372:195.
[59] Liu X, Qiu YL, Ma YT, Zheng HF, Wang LS, Zhang QF, Chen YZ, Peng DL. Facile preparation and microwave absorption properties of porous Co/CoO microrods. J Alloys Compd. 2017;721:411.
[60] Kong J, Wang FL, Wan XZ, Liu JR, Itoh M, Machida K. Template-free synthesis of Co nanoporous structures and their electromagnetic wave absorption properties. Mater Lett. 2012;78:69.
[61] Deng J, Li S, Zhou Y, Liang L, Zhao B, Zhang X, Zhang R. Enhancing the microwave absorption properties of amorphous CoO nanosheet-coated Co (hexagonal and cubic phases) through interfacial polarizations. J Colloid Interface Sci. 2018;509:406.
[62] Liu Q, Xu X, Xia W, Che R, Chen C, Cao Q, He J. Dependency of magnetic microwave absorption on surface architecture of $Co_{20}Ni_{80}$ hierarchical structures studied by electron holography. Nanoscale. 2015;7(5):1736.